ACS APPLIED MATERIALS & INTERFACES

RESEARCH ARTICLE

www.acsami.org

Enhanced Nucleation Rate of Polylactide in Composites Assisted by Surface Acid Oxidized Carbon Nanotubes of Different Aspect Ratios

Zhaohua Xu,[†,§,‡] Yanhua Niu,[‡] Zhigang Wang,[*,†,‡] Heng Li,[§] Liang Yang,[‡] Jie Qiu,[‡] and Howard Wang[⊥]

[†]CAS Key Laboratory of Soft Matter Chemistry, Department of Polymer Science and Engineering, Hefei National Laboratory for Physical Sciences at the Microscale, University of Science and Technology of China, Hefei, Anhui Province 230026, P. R. China

[§]Department of Material Technology, Jiangmen Polytechnic, Jiangmen, Guangdong Province 529090, P. R. China

[‡]Institute of Chemistry, Chinese Academy of Sciences, Beijing 100190, P. R. China

[⊥]Department of Mechanical Engineering, State University of New York at Binghamton, Binghamton, New York 13902, United States

Supporting Information

ABSTRACT: Biodegradable polylactide (PLA) composites added with acid oxidized multiwalled carbon nanotubes (A-MWCNTs) of two different aspect ratios (length to diameter) were prepared by coagulation. The aspect ratios and surface structures of A-MWCNTs were characterized by TGA, Raman, and SEM measurements. The percolation thresholds for gelation in the PLA composites with A-MWCNTs of large and small aspect ratios are 2.5 and 4.0 wt %, respectively, which were determined by a rheological method, and in turn, the rheological result confirms the aspect ratio differences for the added two types of A-MWCNTs in the composites. Isothermal crystallization kinetics of neat PLA and its composites were further investigated by using polarized optical microscope (POM) and differential scanning calorimetry (DSC) to clarify the effects of A-MWCNTs of different aspect ratios and concentrations. The different aspect ratio A-MWCNTs with the same carboxyl group mass percent show substantial effects on PLA crystallization kinetics. Those with smaller aspect ratios enhance nucleation rate for PLA spherulites much more than those with larger aspect ratios. This phenomenon can be attributed to fewer sidewall carboxyl groups on the surfaces of A-MWCNTs with smaller aspect ratios, which provides more nucleation sites for PLA crystallization than those with larger aspect ratios at the same concentration, resulting in faster PLA nucleation rates for the former one.

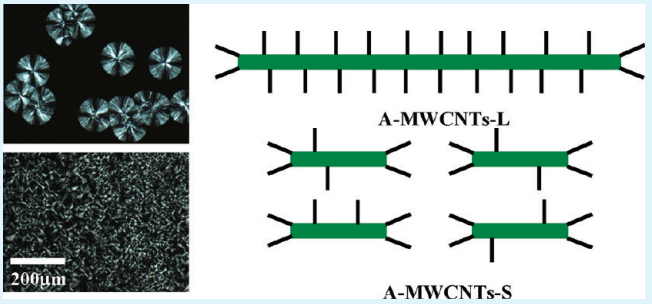

KEYWORDS: polylactide, carbon nanotube, crystallization, aspect ratio

1. INTRODUCTION

Carbon nanotubes (CNTs), since reported by Iijima in 1991, draw increasing interests owing to their unique structures and exciting physical properties.[1] CNTs are used as fillers to incorporate into polymers for the purpose of reinforcement due to their superior mechanical, electrical, and thermal properties.[2−4] The most promising research area on CNT composites focuses on the reinforcement of mechanical properties taking account of the application prospects.[5,6] Besides aiming at improvement of mechanical properties, crystallization behavior of CNT-added polymer composites also attracts much attention because not only the mechanical properties but also the electrical properties considerably depend on the crystalline structures of the polymer matrix.[7] To control crystallization rate and crystallinity to obtain the desired morphology and properties, a great deal of effort has been devoted to study crystallization kinetics and the correlated properties.[8,9] Only small amounts of CNTs added into semicrystalline polymers can accelerate nucleation rate of polymers.[10−13] Valentini and Kumar have found that the availability of nucleation is not linearly proportional to CNT content implying a saturation of the nucleation effect, particularly at a high CNT content.[14,15] In our previous study on CNTs/polypropylene composites, we found an increasing crystallization rate at CNT content below the critical gelation (percolation) concentration, whereas beyond that, the crystallization rates keep independent of CNT content.[16] For some polar polymers, such as nylon 6 and polyethylene oxide, addition of CNTs unexpectedly leads to decreased crystallization rates compared with neat polymers.[8,17] In these cases, the diffusion and alignment of polymer chains into crystal lattices may be retarded by strong interactions between the polar groups of polymers and CNTs, causing decreased crystallization rates.

PLA as a biodegradable polyester has been extensively studied in academic and commercial areas.[18] PLA shows excellent potential for substitution of some petroleum-based polymers

Received: July 17, 2011
Accepted: August 22, 2011
Published: August 22, 2011

due to its favorable biodegradability, producibility from renewable resources, appropriate mechanical properties and versatile fabrication processes.[19] However, the crystallization rate of PLA is relatively slow, which prevents it from developing sufficiently high crystallinity, especially during normal processing conditions involving nonisothermal conditions, such as extrusion and injection molding.[20,21] Accordingly, several technologies, e.g., blending or copolymerization with other polymers, have been developed to improve and/or control the physical properties of PLA.[22−24] Improvement of crystallization rate of PLA is generally achieved through addition of particles such as clays, carbon nanotubes or other inorganic fillers.[25−29] Hu et al. investigated the mechanism of CNTs-induced PLA crystallization by using Fourier transform infrared spectroscopy (FTIR).[30] Their work discloses that PLA chains can be adsorbed on CNTs through the −CH groups, and subsequently PLA backbones make contact with the preadsorbed ones by −(COC + CH_3) interactions to form a unique conformational ordered structure, which finally becomes a precursor of PLA spherulites and causes an increased nucleation rate and the overall crystallization rate.[30] Different crystallization rates induced by pristine CNTs and carboxyl CNTs are considered because of the presence of carboxyl groups for the latter, which partially disables attachment of −CH groups to CNT surface to form the CH−π interaction. The aspect ratio of pristine CNTs is predicted to affect the location of carboxyl groups on the acid oxidized CNTs, that is to say, the locations at the open ends or on the sidewalls, respectively; accordingly, the aspect ratio might affect the crystallization kinetics of PLA. Hitherto, little work has been reported regarding to this aspect.

The objective in this study is to clarify the effects of acid oxidized multiwalled carbon nanotubes (A-MWCNTs) of two different aspect ratios on the crystallization kinetics of PLA. The aspect ratios and surface structures of A-MWCNTs were characterized by TGA, Raman and SEM measurements. A-MWCNTs/PLA composites added with A-MWCNTs of different aspect ratios were first prepared by coagulation. Formation of a jammed network composed of carbon nanotubes is critical to reduce crystallization rate of the composite.[16] Dynamic changes of storage modulus of the PLA composites with different A-MWCNT concentrations were measured to determine the effects of aspect ratio of A-MWCNTs on the network formation in the molten state. Then, the effects of A-MWCNT concentration and aspect ratio on crystallization kinetics of PLA in the composites were investigated by using polarized optical microscopy (POM) and differential scanning calorimetry (DSC). The different aspect ratio A-MWCNTs with the same carboxyl group mass percent showed substantial effects on PLA crystallization kinetics. The nucleation mechanism of different aspect ratio A-MWCNTs for PLA crystallization was finally discussed.

2. EXPERIMENTAL SECTION

Materials. Polylactide (trade name 4032D, NatureWorks China/Hong Kong, Shanghai, China) used in this study was a commercial product with 98.7 mol % L-isomeric content in pellet form, a density of 1.24 g/cm^3, a mass averaged molecular mass of ca. 160 kg/mol and polydispersity of 1.67 (the latter two values were measured by using Waters 2414 GPC, Waters Corporation, USA). Two types of multiwalled carbon nanotubes with large and small aspect ratios were supplied by the ChengDu Organic Chemistry Co. Ltd., Chinese Academy of Sciences (MWCNTs-L, average diameters of 10−20 nm, average length of about 30 μm; MWCNTs-S, average diameters of 10−20 nm, average lengths of 0.5−2 μm; both with special surface area (SSA)>200 m^2/g, with purity >95% and with ash <1.5%). MWCNTs were produced by the chemical vapor deposition method. The other reagents, sulfuric acid (98%), nitric acid (68%), chloroform ($CHCl_3$), and methanol (CH_3OH), were purchased from the Beijing Chemical Reagents Company and were used as received.

MWCNTs-L and MWCNTs-S were respectively mixed with sulfuric acid and nitric acid (3:1 in volume), treated in ultrasonic bath for 1 h, and then refluxed at 60 °C for 4 h to obtain the acid oxidized MWCNTs (A-MWCNTs-L and A-MWCNTs-S). The excess acids were washed thoroughly with deionized water until the pH value was about 7.0. A-MWCNTs were dried in vacuum at 60 °C overnight and then ground to powder in an agate mortar. The carboxyl group mass percents for both A-MWCNTs-L and A-MWCNTs-S were measured by thermogravimetric analysis (Perkin-Elmer 7 TGA analyzer, PerkinElmer, Inc., USA). The sample weights were about 3 mg. The measurements were performed in a flowing nitrogen atmosphere in a temperature range from 50 and 750 °C at a heating rate of 20 °C/min. The lengths of A-MWCNTs-L and A-MWCNTs-S were characterized by using scanning electron microscopy (SEM, Hitachi S-4800, made in Japan). Dilute solutions of A-MWCNTs-L and A-MWCNTs-S obtained by dissolving 0.5 wt % A-MWCNTs-L/PLA and A-MWCNTs-S/PLA composites respectively in chloroform were dropped respectively on clean aluminum foils to form thin films after chloroform evaporated, and the thin films were subjected to SEM observation. For comparison, dilute solutions of A-MWCNTs-L and A-MWCNTs-S in chloroform were dropped respectively on clean aluminum foils to form thin films after chloroform evaporated, and the thin films were subjected to SEM observation as well. Length distributions of A-MWCNTs-L and A-MWCNTs-S could be obtained from these SEM images. An Image Pro Plus software was applied to measure the lengths of A-MWCNTs. Considering the diameters of A-MWCNTs in the range from 10 to 20 nm as reported by the producer, the averaged A-MWCNT aspect ratios could be estimated. Raman spectra of A-MWCNTs-L and A-MWCNTs-S were recorded on a Renishaw-2000 Raman spectrometer (Wotton-under-Edge, Gloucestershire, UK) at a resolution of 2 cm^{-1} by using the 514.5 nm line of an Ar ion laser as the excitation source.

Preparation of A-MWCNTs/PLA Composites. Coagulation was used to prepare A-MWCNTs/PLA composites. Coagulation had been used commonly as an efficient method since it could provide better dispersion of carbon nanotubes in the polymer matrix.[31] First, PLA was dissolved in $CHCl_3$ at room temperature and A-MWCNTs were ultrasonically dispersed in $CHCl_3$ for 1 h. Then, A-MWCNTs/$CHCl_3$ suspension was added into PLA/$CHCl_3$ solution with stirring for 1.5 h to ensure sufficient mixing. Afterward, the suspension was poured into a large amount of cold CH_3OH. After filtration and drying in vacuum at 60 °C for 48 h, an A-MWCNTs/PLA composite could be obtained. A-MWCNTs/PLA composites with different A-MWCNT concentrations ranging from 0 to 8.0 wt % were prepared. Note that A-MWCNTs refer to both of A-MWCNTs-L and A-MWCNTs-S.

Evaluation on Dispersion of A-MWCNTs in A-MWCNTs/PLA Composites. The field-emission scanning electron microscope (FE-SEM, Hitachi S-530, Japan) was used to evaluate the dispersion of A-MWCNTs in the fractured surfaces of the PLA composites. Before SEM observation, the PLA composites were fractured in liquid nitrogen and then the fractured surfaces were sputtered with platinum.

Rheological Measurements on A-MWCNTs/PLA Composites. Rheological measurements were performed on a stress-controlled rheometer (TA-AR2000, TA Instruments, USA) with parallel plates (diameter of 25 mm) in nitrogen atmosphere. Before rheological measurements, the dried A-MWCNTs/PLA composites were pressed in vacuum at 180 °C into disks with thickness of 1 mm and diameter of 25 mm. The samples were further dried in vacuum at 60 °C for 6 h before

the measurements. Oscillatory time sweeps were preformed to ensure that the dried neat PLA and A-MWCNTs/PLA composites did not show obvious storage modulus and viscosity changes for at least 3 h at the testing temperature. Oscillatory frequency sweeps ranging from 0.1 to 500 rad/s with a fixed strain of 0.5% (falling in the linear viscoelasticity regime) were performed at 180 °C for the A-MWCNTs/PLA composites with different A-MWCNT concentrations.

DSC Measurements on Crystallization Kinetics of A-MWCNTs/PLA Composites. DSC (TA-Q200, TA Instruments, USA) was applied to study the crystallization kinetics of A-MWCNTs/PLA composites. All the samples were dried prior to measurements. DSC measurements were performed in nitrogen atmosphere using standard aluminum pans. Prior to the isothermal crystallization kinetics study, the crystallization and melting behaviors during cooling and subsequent heating scans for neat PLA and A-MWCNTs/PLA composites were examined. The samples with ca. 5 mg mass were first heated to 180 °C and held for 5 min to erase thermal histories, then cooled to 30 °C at a cooling rate of 10 °C/min, and finally heated again to 180 °C at a heating rate of 10 °C/min. The isothermal crystallization procedure was designed as follows: the samples were heated from 30 to 180 °C at a rate of 50 °C/min, held at 180 °C for 5 min to erase thermal histories, and then quenched at a rate of 50 °C/min to the desired isothermal crystallization temperatures of 125, 130, 135, and 140 °C, respectively. It should be noticed that normally the optimal temperature (110 °C) for the crystallization kinetic study of PLA from the melt state is lower than the above temperatures we selected (see the Supporting Information). However, at the optimal crystallization temperature plenty of PLA nuclei can form, thus, a very high nucleus density prevents from the optical microscopic observation which we employed in the later section for comparison. For observing the nucleation rate difference induced by different aspect ratio A-MWCNTs, we selected the crystallization temperatures between the optimal temperature and the melting point rather than the optimal temperature.

Optical Microscopic Observation on Nucleation and Spherulite Growth in A-MWCNTs/PLA Composites. The nucleation and growth of spherulites in PLA composites were observed by using POM (Olympus BX51, Japan) equipped with a charge-coupled device (CCD) camera (HV1301UC, Beijing Daheng, China). A homemade dual-temperature hot stage with temperature fluctuations of ±0.1 °C was used to control the sample temperature. The film samples of A-MWCNTs/PLA composites with thickness of about 30 μm, sandwiched between two cover glasses, were first melted at 180 °C for 5 min to erase thermal histories, and then were quickly transferred to the temperatures of 125, 130, 135, and 140 °C for isothermal crystallization, respectively. Note that the samples with A-MWCNT concentrations above 2.0 wt % were too dark to be observed by using POM due to strong light absorption. The sizes of growing spherulites were monitored by taking micrographs at an appropriate time interval before spherulites impinged. Averaged radial growth rates of PLA spherulites (G) were obtained from the slopes of spherulite radius versus time plots.

3. RESULTS AND DISCUSSION

TGA, Raman, and SEM Characterizations of A-MWCNTs-L and A-MWCNTs-S. Figure 1 shows the TGA curves for MWCNTs-L, MWCNTs-S, A-MWCNTs-L and A-MWCNTs-S in nitrogen atmosphere at a heating rate of 20 °C/min. The temperature range from 100 °C up to 500 °C can be used to obtain the carboxyl group mass content on the A-MWCNT surfaces.[32−34] The mass loss at temperatures below 500 °C, which corresponds to the removal of carboxyl groups, offers a direct evidence for the acid oxidization degree (compared with that of MWCNTs-L and MWCNTs-S). Both A-MWCNTs-L and A-MWCNTs-S show the same carboxyl group mass percent

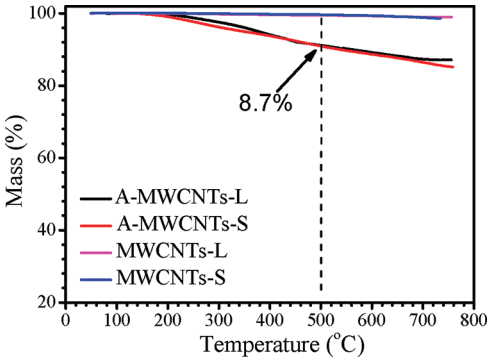

Figure 1. TGA curves of MWCNTs-L, MWCNTs-S, A-MWCNTs-L, and A-MWCNTs-S in nitrogen atmosphere at a heating rate of 20 °C/min.

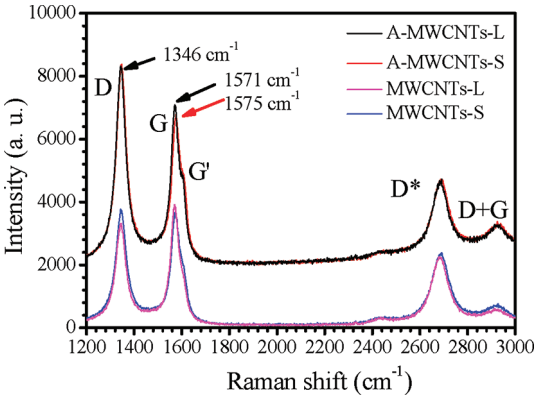

Figure 2. Raman spectra of MWCNTs-L, MWCNTs-S, A-MWCNTs-L, and A-MWCNTs-S for the excitation at 514.5 nm.

of about 8.7 wt %, indicating the same overall oxidization degree for both types of A-MWCNTs. Note that a slightly sharper drop for the A-MWCNTs-S mass from about 200 to 400 °C indicates that the short A-MWCNTs-S decompose at a slightly faster rate than the long A-MWCNTs-L. This is understandable since it has been generally agreed that for oxidized graphites and also for carbon nanotubes more carboxyl groups are mainly situated at the more open ends of the short A-MWCNTs-S and the edges of the tube sheets, causing a relatively faster decomposition rate in comparison with the long A-MWCNTs-L.[33] This result infers that for the short A-MWCNTs-S the carboxyl groups locate relatively more at the open ends while for the long A-MWCNTs-L the carboxyl groups locate relatively more on the sidewalls considering that both A-MWCNTs have the same carboxyl group mass percent.

Figure 2 shows the Raman spectra collected from MWCNTs-L, MWCNTs-S, A-MWCNTs-L and A-MWCNTs-S, respectively. The Raman spectra were acquired at 514.5 nm excitation. It can be seen that the D/G ratio obviously increases for the acid oxidized carbon nanotubes (A-MWCNTs) compared with pristine MWCNTs suggesting an increased density of sp^3-hybridized carbon "defect" sites formed on the A-MWCNT surfaces due to successful acid oxidization. Other important features seen in Figure 2 are the disorder-induced D band at 1346 cm^{-1}, its second harmonic G′ (shoulder in G) at 1603 cm^{-1}, and the tangential G band at 1571 cm^{-1} for A-MWCNTs-L and at 1575 cm^{-1} for A-MWCNTs-S, which is related to the graphite

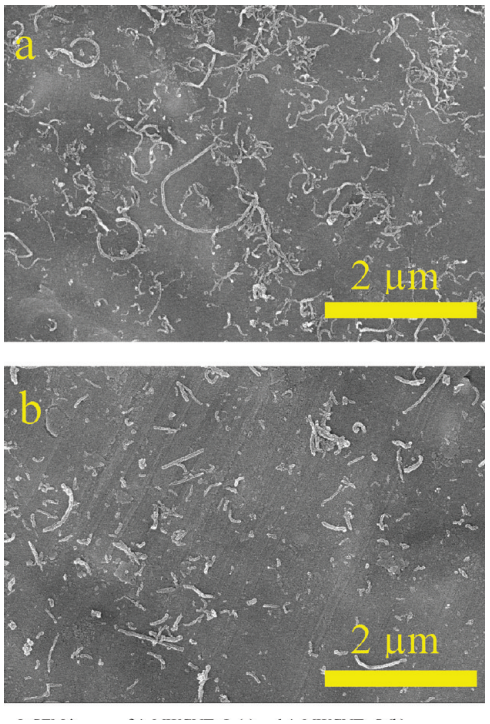

Figure 3. SEM images of (a) A-MWCNTs-L and (b) A-MWCNTs-S.

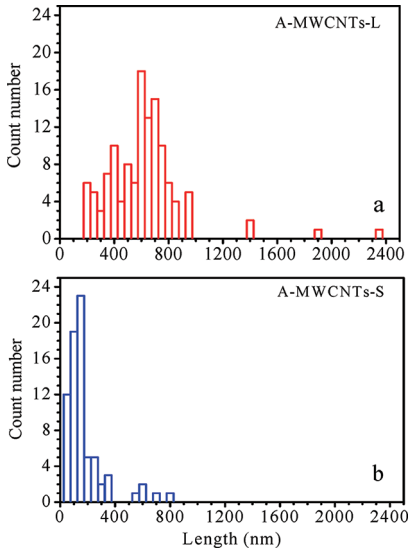

Figure 4. Length distributions of (a) A-MWCNTs-L and (b) A-MWCNTs-S.

tangential E_{2g} Raman active mode where the two atoms in graphene unit cell are vibrating tangentially one against the other. Second order overtone bands (D* and D+G) occur at 2688 and 2926 cm^{-1}, respectively. According to the literature,[33,35] the spectra shown in Figure 2 have been normalized with respect to the second order overtone band D*, indicating slightly different intensities of the G band for the two types of acid oxidized carbon tubes. The slightly higher intensity ratio G/D* for A-MWCNTs-L (1.90) than that for A-MWCNTs-S (1.80) indicates that the G band in the carbon nanotubes is disorder-induced at least in part. As we have inferred from the TGA data,

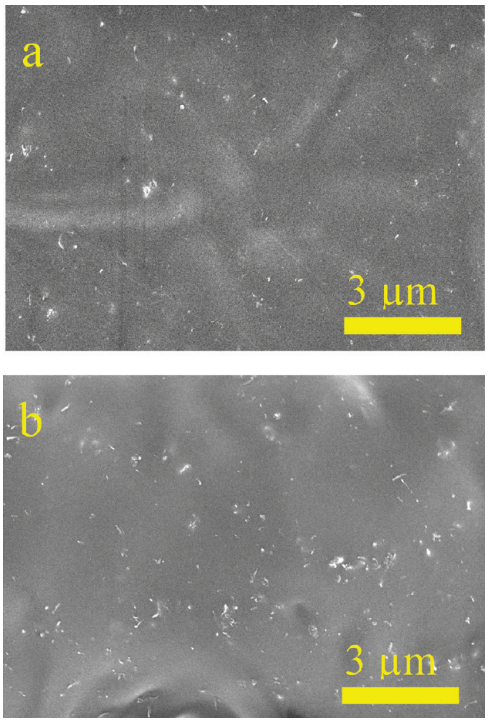

Figure 5. FE-SEM micrographs for 0.5 wt % A-MWCNTs/PLA composites: (a) A-MWCNTs-L/PLA composite and (b) A-MWCNTs-S/PLA composite.

the carboxyl group locates relatively more at the open ends for the short A-MWCNTs-S while the carboxyl group locates relatively more on the sidewalls for the long A-MWCNTs-L considering that both A-MWCNTs have the same carboxyl group mass percent; thus, the defects (grafts of carboxyl group) shall locate more on the sidewalls for the long A-MWCNTs-L, increasing the G band intensity accordingly. In addition, a G band downshift of about 4 cm^{-1} observed in A-MWCNTs-L with respect to A-MWCNTs-S accounts for locations of the carboxyl group on the carbon nanotube surfaces that ultimately decrease more the intrabundle interactions for A-MWCNTs-L than for A-MWCNTs-S. A similar downshift has been proposed for other covalent CNT functionalizations.[36] Location of the carboxyl group on the carbon tubes causes obviously different nucleation rates of PLA as we will show in details in the later sections.

The length distributions of A-MWCNTs obtained from SEM images (Figure 3) are shown in Figure 4. The average lengths of A-MWCNTs-L and A-MWCNTs-S are about 615 and 162 nm, respectively. It can be seen that the carbon nanotube lengths are reduced significantly after acid oxidization because the treatment of pristine MWCNTs with strong oxidizing agents assisted with ultrasonic causes severe etching of the graphitic surfaces of MWCNTs, leading to the tubes of shorter lengths with a large population of disordered sites.[34] The diameters of A-MWCNTs are in a range of 10 to 20 nm as reported by producer, so the average aspect ratios for A-MWCNTs-L and A-MWCNTs-S are 31−62 and 8−16, respectively. We note that the length distributions of A-MWCNTs as obtained from 0.5 wt % A-MWCNTs/PLA composites by dissolving them respectively in $CHCl_3$ were examined and shown in Figures 3 and 4. The length distributions of neat A-MWCNTs films were examined as well for comparison. The results show approximately close

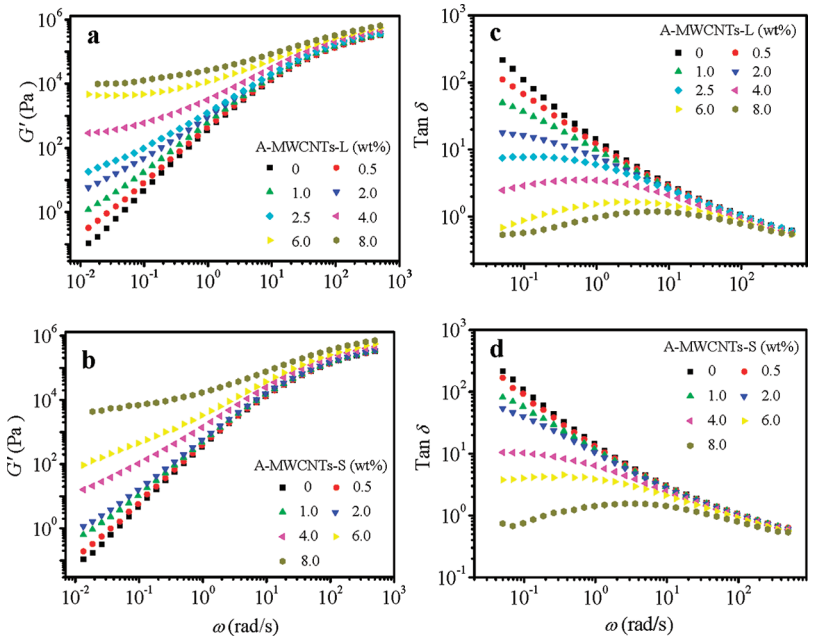

Figure 6. Changes of storage modulus (G') and loss tangent (tan δ) as functions of frequency for A-MWCNTs/PLA with different A-MWCNT concentrations: (a, c) A-MWCNTs-L/PLA composites; and (b, d) A-MWCNTs-S/PLA composites. The rheological measurements were performed with a strain of 0.5% at 180 °C.

length distributions for neat A-MWCNTs films and those obtained from A-MWCNTs/PLA composites (see the Supporting Information).

Dispersion of A-MWCNTs in A-MWCNTs/PLA Composites. Dispersion of MWCNTs in polymers is one of the most important topics for fabricating high performance MWCNTs/polymer composites.[29,36−39] Figure 5 shows the typical FE-SEM images of the fractured surfaces of A-MWCNTs-L/PLA and A-MWCNTs-S/PLA composites with A-MWCNT concentration of 0.5 wt %. The bright regions are attributed to A-MWCNTs due to their high electrical conductivity. It is unambiguous that both A-MWCNTs-L and A-MWCNTs-S are homogeneously dispersed in PLA with no obvious aggregation. It should be mentioned that pristine MWCNTs show obvious heterogeneous dispersion in PLA composites with much large scale MWCNT aggregates, which is not allowed for a comparison study. The homogeneous dispersion of A-MWCNTs in PLA is mainly facilitated by interactions between the functional carboxyl group on A-MWCNT surfaces and PLA chains. Shortening of pristine MWCNT lengths by treatments with strong oxidizing agents and ultrasonic is also thought to be helpful for better dispersion of A-MWCNTs in PLA matrix. Similar results were observed in A-MWCNTs/PLA composites processed by melt mixing.[38,39]

Melt Rheological Behaviors of A-MWCNTs/PLA Composites. Figure 6 shows the changes of storage modulus (G') and loss tangent (tanδ) with frequency for A-MWCNTs-L/PLA and A-MWCNTs-S/PLA composites with different A-MWCNT concentrations at 180 °C in the molten state. At the high frequencies the effect of A-MWCNTs on the rheological behavior is relatively weak, which suggests that A-MWCNTs with much longer relaxation time do not influence the short-range dynamics of PLA chains.[40] At the low frequencies, neat PLA shows a typical response of a viscous material with the scaling property of approximate $G' \propto \omega^2$ indicating a terminal flow behavior. With increasing A-MWCNT concentration, G' at low frequencies increases for both A-MWCNTs-L/PLA and A-MWCNTs-S/PLA composites. At the same A-MWCNT concentration, G' of A-MWCNTs-L/PLA composites is higher than that of A-MWCNTs-S/PLA composites since A-MWCNTs-L have longer relaxation time than A-MWCNTs-S. The interactions between A-MWCNTs and PLA chains slow down the motion of PLA chains. With increasing A-MWCNT concentration, the slope of G' at low frequencies decreases and at a certain concentration overlaps the slope of G'' (data no shown), that is $G' \approx G'' \approx \omega^n$, which indicates a transition from liquidlike to solidlike behaviors.[41,42]

Tan δ can be used as a more sensitive parameter to characterize viscoelasticity and especially the liquid-to-solid transition for polymer composites. For the materials near the liquid-to-solid transition, tan δ decreases with increasing frequency in the pregel regime for a typical viscoelastic liquid. In the postgel regime, a moderate increase in tan δ appears in the low frequency regime indicating an elastic character. At the critical gel point, tan δ becomes independent of frequency because of the intrinsic power law relaxation.[41,42] The frequency dependences of tanδ for A-MWCNTs-L/PLA and A-MWCNTs-S/PLA composites are shown in Figures 6c and 6d. For A-MWCNTs-L/PLA composites tan δ shows evidently a decrease with increasing frequency when A-MWCNTs-L concentration is below 2.5 wt %, indicating a viscous liquid behavior. For A-MWCNTs-S/PLA composites, this concentration locates at 4.0 wt %. Once A-MWCNT concentration is beyond 2.5 wt % for A-MWCNTs-L/PLA composites and beyond 4.0 wt % for A-MWCNTs-S/PLA composites, tanδ drops dramatically at the low frequencies with increasing A-MWCNT concentration. We define the A-MWCNT concentrations of 2.5 wt % and 4.0 wt % as the critical gel concentrations, namely the percolation thresholds, for A-MWCNTs-L/PLA and A-MWCNTs-S/PLA composites, respectively. At these concentrations, plateau regions of tanδ

appear at the low frequencies as a rheological indication of gelation. The percolation threshold can be influenced by MWCNT dispersion, temperature, and more importantly the aspect ratios of MWCNTs.[43−45] In our study the lower percolation threshold value for A-MWCNTs-L/PLA composites than that for A-MWCNTs-S/PLA composites is interpreted by the larger aspect ratios for A-MWCNTs-L than that for A-MWCNTs-S. If taking into account of the above-mentioned factors the values of percolation threshold for A-MWCNTs/PLA composites in this study are in reasonable consistence with that estimated by Bicerano et al.[46] In turn, the above rheological results confirm the aspect ratio differences as observed from SEM for the two types of A-MWCNTs added in the PLA composites.

Effects of A-MWCNTs on Isothermal Crystallization of A-MWCNTs/PLA Composites. Prior to the results and discussion on the isothermal crystallization kinetics, the crystallization and melting behaviors of neat PLA and A-MWCNTs/PLA composites are worth to mention. First, the glass transition temperature of about 60 °C and the melting point of about 165 °C were determined for neat PLA (see the Supporting Information). The DSC heat flow curves for neat PLA and A-MWCNTs/PLA composites during cooling scans (see the Supporting Information) do not show any obvious exothermic peaks indicating the relatively slow crystallization rates for the studied PLA and A-MWCNTs/PLA composites. Three phase transitions, including glass transition, cold crystallization, and melting−recrystallization−remelting, can be clearly observed during the subsequent heating scans. The glass transition temperatures seem less affected by addition of A-MWCNTs. The cold crystallization peak temperature changes following the exactly same trends as that observed during the isothermal crystallization process as shown later in this section, indicating the same effects of addition of A-MWCNTs on the PLA crystallization behaviors. The melting behaviors of A-MWCNTs-L/PLA composites are similar to neat PLA, while the melting behaviors of A-MWCNTs-S/PLA composites with the intermediate A-MWCNTs-S concentrations show multiple melting peaks due to the melting−recrystallization−remelting events, correlating to the faster crystallization rates induced by A-MWCNTs-S. This result is consistent with that observed during the isothermal crystallization process. The key point is that the final melting points remarked by the lines in the figure (see the Supporting Information) are same for all the A-MWCNTs/PLA composites, indicating the melting of PLA lamellar crystals is not affected by addition of A-MWCNTs. This infers that the undercooling for isothermal crystallization at a given crystallization temperature is same for A-MWCNTs/PLA composites, confirming that the isothermal crystallization process of A-MWCNTs/PLA composites at the selected temperatures is mainly nucleation-controlled. The enthalpies of the cold crystallization peak (ΔH_{cc}) and melting peak (ΔH_m) during heating scans (see the Supporting Information) reveal crystallinity values of 32−38% for neat PLA and A-MWCNTs/PLA composites. For the isothermal crystallization kinetics study the PLA composites were quenched at a cooling rate of 50 °C/min from 180 °C to the desired crystallization temperatures, at which the heat flow curves during isothermal crystallization were recorded. The crystallization kinetics is analyzed by using the Avrami equations as follows

$$1 - X(t) = \exp(Kt^n) \quad (1)$$

$$\ln[-\ln(1 - X(t))] = \ln K + n\ln t \quad (2)$$

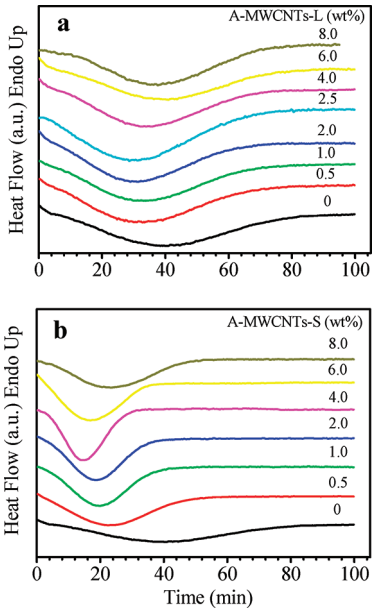

Figure 7. DSC heat flow curves during isothermal crystallization at 130 °C for (a) A-MWCNTs-L/PLA composites and (b) A-MWCNTs-S/PLA composites with different A-MWCNT concentrations.

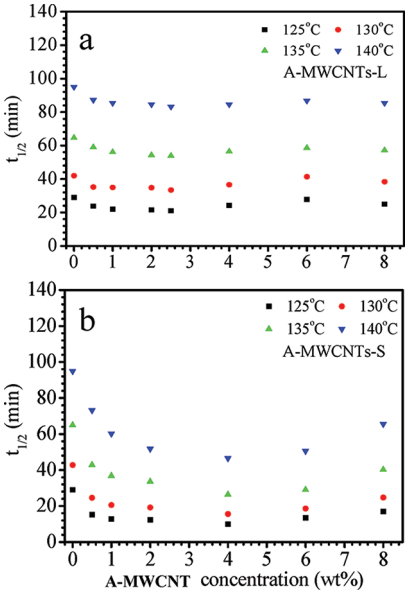

Figure 8. Changes of half crystallization time, $t_{1/2}$, with A-MWCNT concentration at different isothermal crystallization temperatures for (a) A-MWCNTs-L/PLA composites and (b) A-MWCNTs-S/PLA composites.

where $X(t)$ is the relative crystallinity, t the crystallization time, n the Avrami exponent, and K the crystallization rate constant, which depends on the nucleation and growth mechanism of crystallization.[47,48] Half crystallization time ($t_{1/2}$), which represents the crystallization rate, can be obtained from eq 3

$$t_{1/2} = [\ln 2/K]^{1/n} \quad (3)$$

As mentioned in the Experimental Section, the isothermal crystallization of neat PLA and its composites was measured in

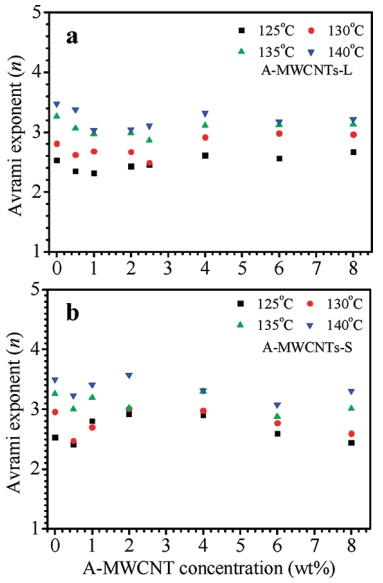

Figure 9. Changes of the Avrami exponent with A-MWCNT concentration at different isothermal crystallization temperatures for (a) A-MWCNTs-L/PLA composites and (b) A-MWCNTs-S/PLA composites.

the temperature range of 125−140 °C. For all the samples, the crystallization process prolongs with increasing crystallization temperature.[49] Figure 7 shows the typical heat flow curves of A-MWCNTs/PLA composites during isothermal crystallization at 130 °C. Compared with neat PLA, loading of both A-MWCNTs-S and A-MWCNTs-L into PLA matrix decreases the peak time of crystallization; however, A-MWCNTs-S/PLA composites at all concentrations show relatively lower peak time values and narrower peak time ranges indicating their faster crystallization rates than that of A-MWCNTs-L/PLA composites. With increasing A-MWCNT concentrations the peak time first shifts to lower values and then shifts back to higher values when beyond certain concentrations. This observation can be demonstrated more clearly by the changes of half crystallization time ($t_{1/2}$), the time required to achieve half of the final crystallinity, which is an important parameter for indication of crystallization kinetics. Figure 8 shows the changes of $t_{1/2}$ with A-MWCNT concentration for these two types of PLA composites. These two types of PLA composites show similar tendency, with $t_{1/2}$ first decreasing to the lowest values until about the percolation concentrations, and then increasing again with even higher concentrations. This tendency is more significant for the composites containing small aspect ratio A-MWCNTs-S. The $t_{1/2}$ value decreases when only 0.5 wt % A-MWCNTs are added indicating an obviously enhanced overall crystallization rates due to nucleating effect of A-MWCNTs. Changes of $t_{1/2}$ also indicate the fastest crystallization rate at 2.5 wt % A-MWCNT concentration for A-MWCNTs-L/PLA composites and at 4.0 wt % for A-MWCNTs-S/PLA composites. When beyond these A-MWCNT percolation concentrations, $t_{1/2}$ values increase and/or keep about constant afterward. The above results indicate that A-MWCNTs serve as nucleating agents to enhance crystallization when below the percolation concentration, but also serve as hindrance to retard crystallization when above the percolation concentration. The latter one is because that the formed A-MWCNT network structure and

Table 1. Crystallization Rate Constant (K) for PLA, A-MWCNTs-L/PLA, and A-MWCNTs-S/PLA Composites at 130 °C

	A-MWCNT concentration (%)							
	0	0.5	1	2	2.5	4	6	8
K_L (min^{-n}) ($\times 10^4$)	0.19	0.50	0.54	0.56	1.07	0.16.	0.14	0.11
K_S (min^{-n}) ($\times 10^4$)	0.19	1.24	1.68	2.17		2.71	2.19	1.63

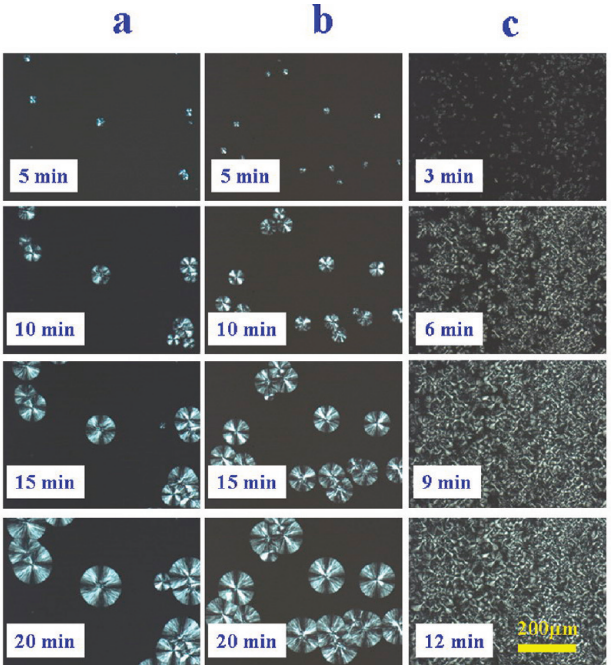

Figure 10. Polarized optical micrographs indicating the nucleation and spherulite growth during isothermal crystallization at 130 °C for (a) neat PLA, (b) 0.5 wt % A-MWCNTs-L/PLA composite, and (c) 0.5 wt % A-MWCNTs-S/PLA composite. The yellow bar in the bottom right micrograph represents 200 μm and is applied to all the micrographs.

the resulted high melt complex viscosity lead to restriction of PLA chain diffusion to an ordered packing state, thus, a decreased crystallization rate is observed. This finding is in accordance with our previous result about the crystallization kinetics of MWCNTs/iPP composites.[16] Furthermore, one can find that the slopes for $t_{1/2}$ versus concentration plots above the percolation thresholds are clearly larger for A-MWCNTs-S/PLA composites, suggesting that the PLA chain diffusion barrier is larger for the composites added with the shorter carbon tubes than that added with the longer carbon tubes.

Plots of $\ln[-\ln(1 - X(t))]$ versus $\ln(t)$ for A-MWCNTs/PLA composites isothermally crystallized at different temperatures show linear relationships, from which the Avrami exponents can be obtained from slopes of the fitted lines. Variations of the Avrami exponent with A-MWCNT concentration for A-MWCNTs/PLA composites crystallized at different temperatures are shown in Figure 9. The average values of n are close to 3 for the PLA composites indicating that PLA crystallizes mostly through heterogeneous nucleation followed by three-dimensional spherulite growth.[29,50,51] The average slightly increased n values

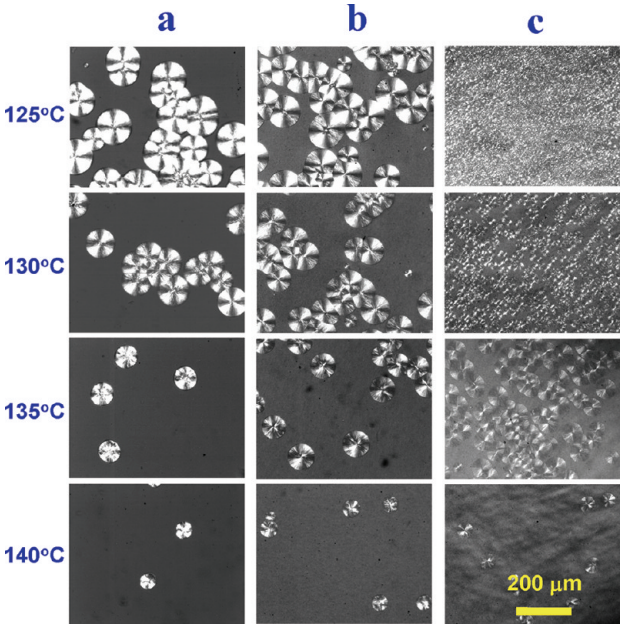

Figure 11. Polarized optical micrographs indicating the nucleation and spherulite growth during isothermal crystallization at different temperatures for (a) neat PLA of 30 min crystallization time, (b) 0.5 wt % A-MWCNTs-L/PLA composite of 30 min and (c) 0.5 wt % A-MWCNTs-S/PLA composite of 15 min. The yellow bar in the bottom right micrograph represents 200 μm and is applied to all the micrographs.

Table 2. Numbers of Nuclei Counted for PLA, A-MWCNTs-L/PLA (0.5 wt % A-MWCNTs-L) and A-MWCNTs-S/PLA (0.5 wt % A-MWCNTs-S) at different crystallization temperatures

T (°C)	PLA	A-MWCNTs-L/PLA	A-MWCNTs-S/PLA
125	20	26	too many to count
130	13	24	442
135	4	12	103
140	2	5	11

(up to 3.5) with increasing isothermal temperature indicate appearance of some homogeneous nucleation for PLA at the higher crystallization temperature. The heterogeneous nucleation for PLA is more significant at the lower crystallization temperature. The DSC results reported here are consistent with PLA spherulitic morphology, which will be shown in the following section. The crystallization rate constant K values for neat PLA and A-MWCNTs/PLA composites with different A-MWCNT concentrations at 130 °C are listed in Table 1. For the given crystallization temperature, the crystallization rate constant increases with addition of A-MWCNTs as compared with neat PLA indicating that the PLA crystallization process is nucleation-controlled because A-MWCNTs function as heterogeneous nucleating agents. Moreover, the K values are higher for A-MWCNTs-S/PLA composites than A-MWCNTs-L/PLA composites, indicating that A-MWCNTs-S are more efficient nucleating agents for enhancing PLA crystallization rate than A-MWCNTs-L. The different K values for A-MWCNTs/PLA composites are attributed to both the heterogeneous nucleation ability of A-MWCNTs for PLA crystallization and diffusion

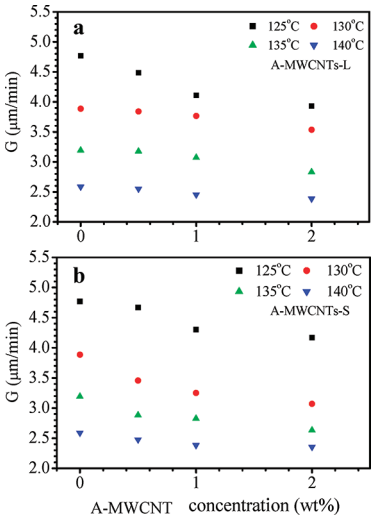

Figure 12. Changes of radial growth rate of spherulites as functions of A-MWCNT concentration at different crystallization temperatures for (a) A-MWCNTs-L/PLA composites and (b) A-MWCNTs-S/PLA composites.

retardation to PLA chains from the formed network constraint of A-MWCNTs at the higher A-MWCNT concentrations.

Nucleation and Spherulite Growth during Isothermal Crystallization of A-MWCNTs/PLA Composites. Typical polarized optical micrographs of spherulites imaged during the crystallization process of PLA and PLA composites containing 0.5 wt % A-MWCNTs-L and A-MWCNTs-S at 130 °C for different time are shown in Figure 10. Typical polarized optical micrographs of spherulites imaged during the crystallization process of PLA and PLA composites containing 0.5 wt % A-MWCNTs-L and A-MWCNTs-S at different temperatures for certain times are shown in Figure 11. Table 2 lists numbers of nuclei counted for PLA, A-MWCNTs-L/PLA (0.5 wt % A-MWCNTs-L) and A-MWCNTs-S/PLA (0.5 wt % A-MWCNTs-S) at different crystallization temperatures. It can be easily seen that addition of A-MWCNTs accelerates nucleation of PLA dramatically when comparing with neat PLA. Moreover, nucleating ability of A-MWCNTs-S is obviously much more significant than that of A-MWCNTs-L. Comparing PLA with A-MWCNTs-L/PLA composite, the average spherulite diameters remain about similar, whereas for A-MWCNTs-S/PLA composite, the nuclei burst so much that it is difficult to distinguish individual spherulites.[28] The above result indicates that not all of the nanotubes play the role of nucleating agent, because in that case, many more spherulites should be observed than shown in Figures 10 and 11. Heterogeneous nucleation effect of A-MWCNTs for PLA at the low temperatures is more apparent, thus, the nucleation ability of A-MWCNTs-S is more significant than A-MWCNTs-L at the low temperatures. One may predict that A-MWCNTs-S with the same mass amount in the PLA matrix as A-MWCNTs-L has about four times the tube ends of A-MWCNTs-L (considering approximately its four times tube length), thus, A-MWCNTs-S should show about four times the nucleation ability of A-MWCNTs-L, however, the number of nuclei listed in Table 2 at 130 °C for A-MWCNTs-S/PLA is about eighteen times of that for A-MWCNTs-L/PLA. The above result cannot be simply explained only by the aspect ratio difference. We will provide a reasonable explanation in the

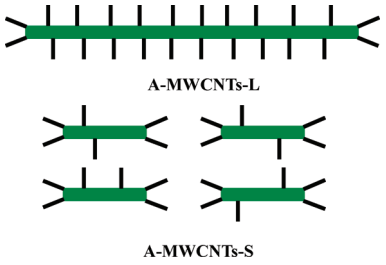

Figure 13. Schematics of A-MWCNTs-L and A-MWCNTs-S. The green bars represent the MWCNTs of different aspect ratios (four times used here) and the black lines represent the grafted carboxyl groups.

nucleation mechanism section by considering the distribution of carboxyl group on the carbon nanotubes associated with the tube aspect ratio and the FTIR experimental evidence from the literature.[30]

The 1.0 and 2.0 wt % composite samples were also examined at different temperatures for obtaining the radial growth rates of spherulites. Figure 12 shows the radial growth rates of PLA spherulites at various temperatures for neat PLA and the composites containing 0.5, 1.0, and 2.0 wt % of A-MWCNTs. The decreasing G with increasing temperature is consistent with the nucleation-controlled crystal growth mechanism. G decreases with increasing A-MWCNT concentration at each crystallization temperature because of increasing viscosity of A-MWCNTs/PLA composites and accordingly decreasing diffusion rate of PLA chains for crystal growth. Obviously the energy barrier for transport of PLA chains in the undercooled melt increases with increasing A-MWCNT concentration. At the low isothermal crystallization temperatures G decreases significantly with increasing A-MWCNT concentration, indicating more obvious effect of the energy barrier for transport of PLA chains to crystal growth fronts; while at the high isothermal crystallization temperatures, such an effect of energy barrier is largely weakened.[52] The slopes for G versus concentration plots are relatively larger (corresponding to the relatively lower G values) for A-MWCNTs-S/PLA composites, suggesting that the PLA chain diffusion barrier is larger for the composites added with the shorter carbon tubes than that added with the longer carbon tubes, consistent with the changes of $t_{1/2}$ versus concentration plots. Nevertheless, comparing G values of the composites containing the same concentration of A-MWCNTs-L and A-MWCNTs-S at the same crystallization temperature the differences are not obvious, which demonstrates that addition of A-MWCNTs mainly affects nucleation rate for PLA crystallization at low A-MWCNT concentrations.

Nucleation Mechanism for Isothermal Crystallization of A-MWCNTs/PLA Composites. The above results clearly demonstrate that A-MWCNTs-S with small aspect ratios can induce a fast nucleation rate for PLA crystallization, while the A-MWCNTs-L with large aspect ratios induces a slow nucleation rate for PLA crystallization. The difference can be well explained as follows. Computer simulation results indicate that polymer backbones provide the strongest binding to nanotubes rather than the side groups.[53] Adsorption of PLA on CNTs can be attributed to the CH-π interaction between PLA backbone and CNTs, and then successive −CH groups gradually attach themselves to CNT surface.[30] Therefore, efficiency of adsorption depends on the number of −CH group and the available A-MWCNT surfaces for molecular interactions. According to the TGA, Raman, and SEM results, the A-MWCNT surface structures can be schematically described in Figure 13, given that both A-MWCNTs-L and A-MWCNTs-S have the same carboxyl group content by TGA measurement, the different aspect ratios (difference of four times is applied here for simplicity) by SEM observation and different locations of grafted carboxyl groups on the A-MWCNT surfaces by Raman and TGA measurements. It can be seen that for the same A-MWCNT concentration in the PLA composites, A-MWCNTs-L have less carboxyl groups on the open ends and correspondingly more carboxyl groups on the sidewalls than A-MWCNTs-S under the same total length condition, assuming close densities and tube diameters for these two types of carbon nanotubes. Hu et al. made a clear conclusion from their FTIR studies that the carboxyl groups on the sidewalls of carbon nanotubes inhibit nucleation significantly.[30] From this viewpoint, it is considered that the lower nucleation rate of A-MWCNTs-L than A-MWCNTs-S in the PLA composites can be mainly ascribed to the much more dense location of grafted carboxyl groups on the sidewalls of A-MWCNTs-L than A-MWCNTs-S. Our POM and DSC results in this study on PLA crystallization kinetics in the composites added with acid oxidized carbon nanotubes of two different aspect ratios strongly support the previous conclusion made from the FTIR studies about the nucleation mechanism of acid oxidized carbon nanotubes for PLA component.[30] In addition, it is predicted that the length distribution of A-MWCNTs could have a secondary effect on the results we have observed. A-MWCNTs-S show a narrower length distribution, which could also enhance the nucleation rate. Further study is certainly necessary for confirming this prediction.

4. CONCLUSIONS

The effects of acid oxidized A-MWCNTs with different aspect ratios on the crystallization kinetics of PLA in the composites have been investigated through DSC measurements and POM observation. The aspect ratios and surface structures of A-MWCNTs were characterized by TGA, Raman and SEM measurements. Rheological measurements reveal percolation concentrations for gelation are about 2.5 wt % for the PLA composites added with large aspect ratio A-MWCNTs-L and 4.0 wt % for the PLA composites added with small aspect ratio A-MWCNTs-S, and in turn, the rheological result confirms the aspect ratio differences for the added two types of A-MWCNTs in PLA composites. The A-MWCNT concentrations present different effects on PLA crystallization in that A-MWCNTs first promote crystallization when the A-MWCNT concentration is below the percolation value, and then restrain crystallization through the formed A-MWCNT network structure when the A-MWCNT concentration is beyond the percolation value. Isothermal crystallization results from DSC measurements show that the half crystallization time of A-MWCNTs/PLA composites is significantly reduced with addition of A-MWCNTs and the Avrami exponent related to the dimensionality of crystal structure is about 3 for A-MWCNTs/PLA composites and neat PLA. POM observation shows that addition of A-MWCNTs increases nucleation density of PLA more significantly for the composites containing A-MWCNTs-S than that containing A-MWCNTs-L because A-MWCNTs-S sidewalls supply more nucleating sites than that A-MWCNTs-L. Acid oxidized A-MWCNTs of different aspect ratios do not show obvious effect on the radial growth rates of PLA spherulites. Our results

strongly support the conclusion that the grafted carboxyl groups on A-MWCNT sidewalls inhibit the A-MWCNT nucleation ability for PLA crystallization in the composites.

■ ASSOCIATED CONTENT

Supporting Information. DSC heat flow curves during cooling and heating scans for neat PLA and A-MWCNTs/PLA composites, crystallization rate for neat PLA at different temperatures, SEM images for neat A-MWCNT films and length distributions for neat A-MWCNTs. This material is available free of charge via the Internet at http://pubs.acs.org.

■ AUTHOR INFORMATION

Corresponding Author
*Tel.: +86 0551-3607703. Fax: +86 0551-3607703. E-mail: zgwang2@ustc.edu.cn (Z.G.W.).

■ ACKNOWLEDGMENT

Z.G.W. acknowledges the financial support from the National Science Foundation of China with Grant 51073145.

■ REFERENCES

(1) Iijima, S. *Nature* **1991**, *354*, 56.
(2) Seo, M. K.; Park, S. J. *Chem. Phys. Lett.* **2004**, *395*, 44.
(3) Jiang, X. W.; Bin, Y. Z.; Matsuo, M. *Polymer* **2005**, *46*, 7418.
(4) Kim, Y. A.; Kamio, S.; Tajiri, T.; Hayashi, T.; Song, S. M.; Endo, M.; et al. *Appl. Phys. Lett.* **2007**, *90*, 093125.
(5) Wang, S. F.; Shen, L.; Zhang, W. D.; Tong, Y. J. *Biomacromolecules* **2005**, *6*, 3067.
(6) Liu, T. X.; Phang, I. Y.; Shen, L.; Chow, S. Y.; Zhang, W. D. *Macromolecules* **2004**, *37*, 7214.
(7) Corradini, P.; Guerra, G. *Adv. Polym. Sci.* **1992**, *100*, 183.
(8) Li, J.; Fang, Z. P.; Tong, L. F.; Gu, A. J.; Liu, F. *Eur. Polym. J.* **2006**, *42*, 3230.
(9) Di Lorenzo, M. L.; Silvestre, C. *Prog. Polym. Sci.* **1999**, *24*, 917.
(10) Anand, K. A.; Agarwal, U. S.; Joseph, R. *Polymer* **2006**, *47*, 3976.
(11) Chen, J. H.; Yao, B. X.; Su, W. B.; Yang, Y. B. *Polymer* **2007**, *48*, 1756.
(12) Assouline, E.; Lustiger, A.; Barber, A. H.; Cooper, C. A.; Klein, E.; Wachtel, E.; et al. *J. Polym. Sci., Part B: Polym. Phys.* **2003**, *41*, 520.
(13) Shieh, Y. T.; Twu, Y. K.; Su, C. C.; Lin, R. H.; Liu, G. L. *J. Polym. Sci., Part B: Polym. Phys.* **2010**, *48*, 983.
(14) Valentini, L.; Biagiotti, J.; Kenny, J. M.; Santucci, S. *J. Appl. Polym. Sci.* **2003**, *87*, 708.
(15) Kumar, S.; Doshi, H.; Srinivasarao, M.; Park, J. O.; Schiraldi, D. A. *Polymer* **2002**, *43*, 1701.
(16) Xu, D. H.; Wang, Z. G. *Polymer* **2008**, *49*, 330.
(17) Chatterjee, T.; Yurekli, K.; Hadjiev, V. G.; Krishnamoorti, R. *Adv. Funct. Mater.* **2005**, *15*, 1832.
(18) Ray, S. S.; Bousmina, M. *Prog. Mater. Sci.* **2005**, *50*, 962.
(19) Pan, P.; Kai, W.; Zhu, B.; Dong, T.; Inoue, Y. *Macromolecules* **2007**, *40*, 6898.
(20) Li, Y. L.; Wang, Y.; Liu, L.; Han, H.; Xiang, F. M.; Zhou, Z. W. *J. Polym. Sci., Part B: Polym. Phys.* **2009**, *47*, 326.
(21) Urayama, H.; Kanamori, T.; Kimura, Y. *Macromol. Mater. Eng.* **2001**, *286*, 705.
(22) Yu, T. L.; Huang, B. H.; Hung, W. C.; Lin, C. C.; Wang, T. C.; Ho, R. M. *Polymer* **2007**, *48*, 4401.
(23) Focarete, M. L.; Gazzano, M.; Scandola, M.; Kumar, A.; Gross, R. A. *Macromolecules* **2002**, *35*, 8066.
(24) Lopez-Rodriguez, N.; Lopez-Arraiza, A.; Meaurio, E.; Sarasua, J. R. *Polym. Eng. Sci.* **2006**, *46*, 1299.
(25) Krikorian, V.; Pochan, D. J. *Macromolecules* **2004**, *37*, 6480.
(26) Shieh, Y. T.; Liu, G. L. *J. Polym. Sci., Part B: Polym. Phys.* **2007**, *45*, 1870.
(27) Zhao, Y. Y.; Qiu, Z. B.; Yang, W. T. *Compos. Sci. Technol.* **2009**, *69*, 627.
(28) Xu, H. S.; Dai, X. J.; Lamb, P. R.; Li, Z. M. *J. Polym. Sci., Part B: Polym. Phys.* **2009**, *47*, 2341.
(29) Zhao, Y. Y.; Qiu, Z. B.; Yang, W. T. *J. Phys. Chem. B* **2008**, *112*, 16461.
(30) Hu, X.; An, H. N.; Li, Z. M.; Geng, Y.; Li, L. B.; Yang, C. L. *Macromolecules* **2009**, *42*, 3215.
(31) Du, F. M.; Fisher, J. E.; Winey, K. I. *J. Polym. Sci., Part B: Polym. Phys.* **2003**, *41*, 3333.
(32) Andersson, C. H.; Grennberg, H. *Eur. J. Org. Chem.* **2009**, 4421.
(33) Murphy, H.; Papakonstantinou, P.; Okpalugo, T. I. T. *J. Vac. Sci. Technol. B* **2006**, *24*, 715.
(34) Datsyuk, V.; Kalyva, M.; Papagelis, K.; Parthenios, J.; Tasis, D.; Siokou, A.; Kallitsis, I.; Galiotis, C. *Carbon* **2008**, *46*, 833–840.
(35) Maultzsch, J.; Reich, S.; Thomsen, C.; Webster, S.; Czerw, R.; Carroll, D. L.; Vieira, S. M. C.; Birkett, P. R.; Rego, C. A. *Appl. Phys. Lett.* **2002**, *81*, 2647.
(36) Giambastiani, G.; Cicchi, S.; Giannasi, A.; Luconi, L.; Rossin, A.; Mercuri, F.; Bianchini, C.; Brandi, A.; Melucci, M.; Ghini, G.; Stagnaro, P.; Conzatti, L.; Passaglia, E.; Zoppi, M.; Montini, T.; Fornasiero, P. *Chem. Mater.* **2011**, *23*, 1923.
(37) Chen, G. X.; Kim, H. S.; Park, B. H.; Yoon, J. S. *Polymer* **2006**, *47*, 4760.
(38) Villmow, T.; Potschke, P.; Pegel, S.; Haussler, L.; Kretzschmar, B. *Polymer* **2008**, *49*, 3500.
(39) Wu, D. F.; Wu, L.; Zhang, M.; Zhao, Y. L. *Polym. Degrad. Stab.* **2008**, *93*, 1577–1584.
(40) Mitchell, C. A.; Bahr, J. L.; Arepalli, S.; Tour, J. M.; Krishnamoorti, R. *Macromolecules* **2002**, *35*, 8825.
(41) Winter, H. H.; Mours, M. Rheology of Polymers Near Liquid−Solid Transitions. In *Neutron Spin Echo Spectroscopy, Viscoelasticity, Rheology*; Advances in Polymer Science; Springer: New York, 1997; Vol. 134, p 165
(42) Potschke, P.; Abdel-Goad, M.; Alig, I.; Dudkin, S.; Lellinger, D. *Polymer* **2004**, *45*, 8863.
(43) Li, J.; Ma, P. C.; Chow, W. S.; To, C. K.; Tang, B. Z.; Kim, J. K. *Adv. Funct. Mater.* **2007**, *17*, 3207.
(44) Fredrickson, G. H.; Bicerano, J. *J. Chem. Phys.* **1999**, *110*, 2181.
(45) Wu, D. F.; Wu, L.; ZHOU, W. D.; Sun, Y. R.; Zhang, M. *J. Polym. Sci., Part B: Polym. Phys.* **2010**, *48*, 479–489.
(46) Bicerano, J.; Douglas, J. F.; Brune, D. A. *J. Macromol. Sci.* **1999**, *C39*, 561.
(47) Avrami, M. *J. Chem. Phys.* **1939**, *7*, 1103.
(48) Avrami, M. *J. Chem. Phys.* **1941**, *9*, 177.
(49) Xu, J. T.; Zhao, Y. Q.; Wang, Q.; Fan, Z. Q. *Polymer* **2005**, *46*, 11978.
(50) Wu, D. F.; Wu, L.; Zhou, W. D.; Zhang, M; Yang, T. *Polym. Eng. Sci.* **2010**, *50*, 1721–1733.
(51) He, Y.; Fan, Z. Y.; Hu, Y. F.; Wu, T.; Wei, J.; Li, S. M. *Eur. Polym. J.* **2007**, *43*, 4431.
(52) Avella, M.; Cosco, S.; Volpe, G. D.; Errico, M. E. *Adv. Polym. Technol.* **2005**, *24*, 132.
(53) Panhuis, M. I. H.; Maiti, A.; Dalton, A. B.; van den Noort, A.; Coleman, J. N.; McCarthy, B.; Blau, W. J. *J. Phys. Chem. B* **2003**, *107*, 478.